SUPPLEMENTAL INFORMATION

An intrinsically disordered peptide from Ebola virus VP35 controls viral RNA synthesis by modulating nucleoprotein-RNA interactions

Daisy W. Leung[1#], Dominika M. Borek[2#], Priya Luthra[3], Jennifer M. Binning[1], Manu Anantpadma[4], Gai Liu[1], Ian B. Harvey[1], Zhaoming Su[5], Ariel Endlich-Frazier[3], Juanli Pan[1], Reed S. Shabman[3], Wah Chiu[5], Robert Davey[4], Zbyszek Otwinowski[2], Christopher F. Basler[3], and Gaya K. Amarasinghe[1*]

[1]Department of Pathology and Immunology, Washington University School of Medicine, St Louis, MO 63110, United States

[2]Departments of Biophysics and Biochemistry, University of Texas Southwestern Medical Center at Dallas, TX 75390, United States

[3]Department of Microbiology, Icahn School of Medicine at Mount Sinai, New York, NY 10029, United States

[4]Department of Virology and Immunology, Texas Biomedical Research Institute, San Antonio, TX 78227, United States

[5]National Center for Macromolecular Imaging, Baylor College of Medicine, Houston, TX 77030, United States

#co-first authors

[*]corresponding author

SUPPLEMENTAL TABLE LEGEND

Table S1, related to Figure 2. Data collection, refinement and validation statistics. Summary of data collection, refinement, and validation statistics for the ΔNP_{NTD}/NPBP complex.

SUPPLEMENTAL FIGURE LEGENDS

Figure S1. Sequence alignments of ebolavirus NP and VP35 genes, related to Figure 1 and 2. (**A**) Sequence alignment of ebolavirus nucleoprotein molecules. Sequences were aligned using ClustalW. Accession numbers used in this alignment are AAD14590.1, NC006432.1, YP003815432, YP003815423 and NP690580 for Ebola virus, Sudan virus, Bundibugyo virus, Taï Forest virus, and Reston virus, respectively. Secondary structural elements from PDB 4QB0 were included in the output. Corresponding Western blots for results shown in (**B**) Figure 1E and (**C**) Figure 1F. (**D**) Sequence alignment of ebolavirus VP35 proteins. Sequences were aligned using ClustalW. Accession numbers used in this alignment are AAD14590.1, ACR33188, ACI28621, ACI28630 and BAB69004 for ebolavirus, Sudan virus, Bundibugyo virus, Taï Forest virus, and Reston virus, respectively. Secondary structure elements from PDB 3FKE were included in the output. Residues conserved across all ebolaviruses are colored red; partially conserved are colored pink; those not conserved are not highlighted.

Figure S2. ΔNP_{NTD} and VP35 peptide forms a 1:1 complex in solution, related to Figure 2 and 3. (**A**) Pulldown assay showing binding between VP35 N-terminus and ΔNP_{NTD}. MBP-tagged VP35 1-168 was prebound on amylose resin (bound beads, BB) prior to the addition of ΔNP_{NTD} (input, I). Shown are the final beads (FB) after 3 washes

(W). (**B**) ITC studies show that VP35 NPBP binds with high affinity to ΔNP_{NTD}. A representative raw ITC data and corresponding binding isotherm for ΔNP binding to VP35 peptide are shown. Representative data is from at least 2-4 independent experiments. (**C**) Summary of EBOV VP35 peptide analysis. Shown are the results from ITC and CD measurements. (**D**) Representative CD measurements monitoring the mean residue ellipticity for EBOV peptides described in (**B**) in the absence (dotted lines) or presence of 50% TFE (solid lines). (**E**) Analysis by SEC-MALS shows that the NPBP/ΔNP_{NTD} complex elutes with a molecular mass of 50 ± 0.2 kDa, indicating one molecule of ΔNP_{NTD} with one NPBP. Data shown is representative from at least two independent experiments.

Figure S3. The asymmetric unit of the NPBP/ΔNP_{NTD} complex contains four complexes with 1:1 stoichiometry, related to Figures 2, 3, and 4. (**A**) The individual NPBP/ΔNP_{NTD} complexes are shown in yellow/orange (mol A/mol E), magenta/blue (mol B/mol F), green/purple (mol C/mol G), and cyan/pink (mol D/mol H). The asymmetric unit is shown in three different orientations to highlight how two NPBP/ΔNP_{NTD} complexes of the asymmetric unit (e.g. mol A/mol E and mol C/mol G) form the subunits for one octameric ring, shown in (**B**) Only NP residues 37-385 and VP35 residues 20-47 were modeled in the final refined structure. (**C**) Surface and ribbon representation of three assembled NP molecules in the octameric ring (see (**B**) dotted line) highlighting the foot lobe interaction between adjacent NP molecules. (**D**) 2mFo-DFc maps for representative fragments of the NP molecule head and foot lobes. The electron density maps gradually lose the atomicity with the increasing B-factors for the head lobe, while the foot lobe atomicity is preserved for all chains (also see **Table S1**).

Figure S4. Topological diagram of the structures of ΔNP_{NTD} and VP35 NPBP, related to Figure 2, 3, and 4. (**A**) ΔNP_{NTD} contains a head lobe that is connected to a foot lobe through a hinge region (α7-α12). (**B**) VP35 NPBP forms a short alpha helix and a 3_{10} helix.

Figure S5. MG assay results and TAT-NPBP cell toxicity shows the protein expression for respective MG assay, related to Figure 6. (**A-C**) Corresponding Western blots for results shown in Figure 6 panels (**A**), (**B**), and (**C**), respectively. (**D**) Growth inhibition analysis for Tat-NPBP peptides reveal no significant cytotoxicity. 293T cells (1250 cells/well) were plated in a 96-well plate. Next day, the cells were treated with peptides, control or TAT-NPBP at 3-fold dilutions. 20h later cell toxicity was analyzed using CellTiter-Glo® (Promega) substrate. In this assay, percent inhibition of minigenome activity is calculated by normalizing with negative (untreated sample) sample.

Figure S6. Comparison of Ebola virus NP with N proteins from NNSV family members VSV and NiV, related to Figure 6. Structural alignment of NPBP/ΔNP_{NTD} complex (green/purple) with (**A**) VSV N^0/P complex (cyan/orange, PDB 3PMK) and (**B**) Nipah virus N^0/P complex (orange/blue, PDB 3CO6) show structural differences between the nucleoprotein molecules and peptide binding sites. (**C**) Table of structural alignments of Ebola virus NPBP/ΔNP_{NTD} with other NNSV N^0/P protein complexes.

Table S1. Data collection and refinement statistics

Data collection			
Number of crystals	3[a]		
Space group	F222		
Resolution range (Å)	25.00-3.70 (3.72-3.70)		
Crystal	1	2	3
Wavelength (Å)	0.97913	0.98792	0.98792
Cell dimensions *a, b, c* (Å)	149.6, 195.0, 347.0	148.6, 193.9, 345.7	149.7, 194.8, 347.7
Number of unique reflections	26,688 (1299)[b]	26,497 (1296)	27,102 (1214)
Completeness (%)	99.8 (100.0)	99.7 (99.8)	99.3 (88.8)
Redundancy	6.0 (5.9)	5.7 (5.5)	9.6 (6.6)
$\langle I \rangle / \langle \sigma(I) \rangle$[c]	17.2/0.9	16.6/0.5	30.0/0.1
Anisotropic resolution [Å]	3.9 II a 4.0 II b 3.7 II c	4.1 II a 4.3 II b 3.7 II c	3.9 II a 4.1 II b 3.7 II c
R_{merge}[d]	7.6/NA	6.9/NA	6.8/NA
CC1/2 in the last shell	0.415	0.350	0.551
Refinement			
Resolution (Å)	173.84-3.71 (3.80-3.71)		
Number of reflections (test set)	21,989 (1164)		
R_{work}/R_{free} [%]	25.2/28.5 (34.6/36.7)		
Number of non-H atoms	11,772		
Mean B factor (Å^2)			
• Chain A (NP)	122		
• Chain B (NP)	187		
• Chain C (NP)	88		
• Chain D (NP)	233		
• Chain E (peptide)	88		
• Chain F (peptide)	99		
• Chain G (peptide)	68		
• Chain H (peptide)	126		
R.m.s deviations			
• Bond lengths (Å)	0.006		
• Bond angle (°)	1.019		
Molprobity score[e]	2.21 [100% percentile]		
Molprobity clashscore	4.32 [100% percentile]		

[a] Data from three crystals have been used with merging performed at the level of .sca files rather than reflection files, therefore statistics corresponding to each .sca file are provided.

[b] Data for the highest resolution shell are shown in parenthesis.

[c] Crystals diffracted anisotropically. The correction for anisotropy was applied during scaling data with Scalepack.

[d] R_{merge} higher than 1 is statistically meaningless, therefore Scalepack (Minor, 1997)) does not report it.

[e] Carried out using MolProbity (Chen et al., 2010).

Figure S1, related to Figure 1 and 2

A

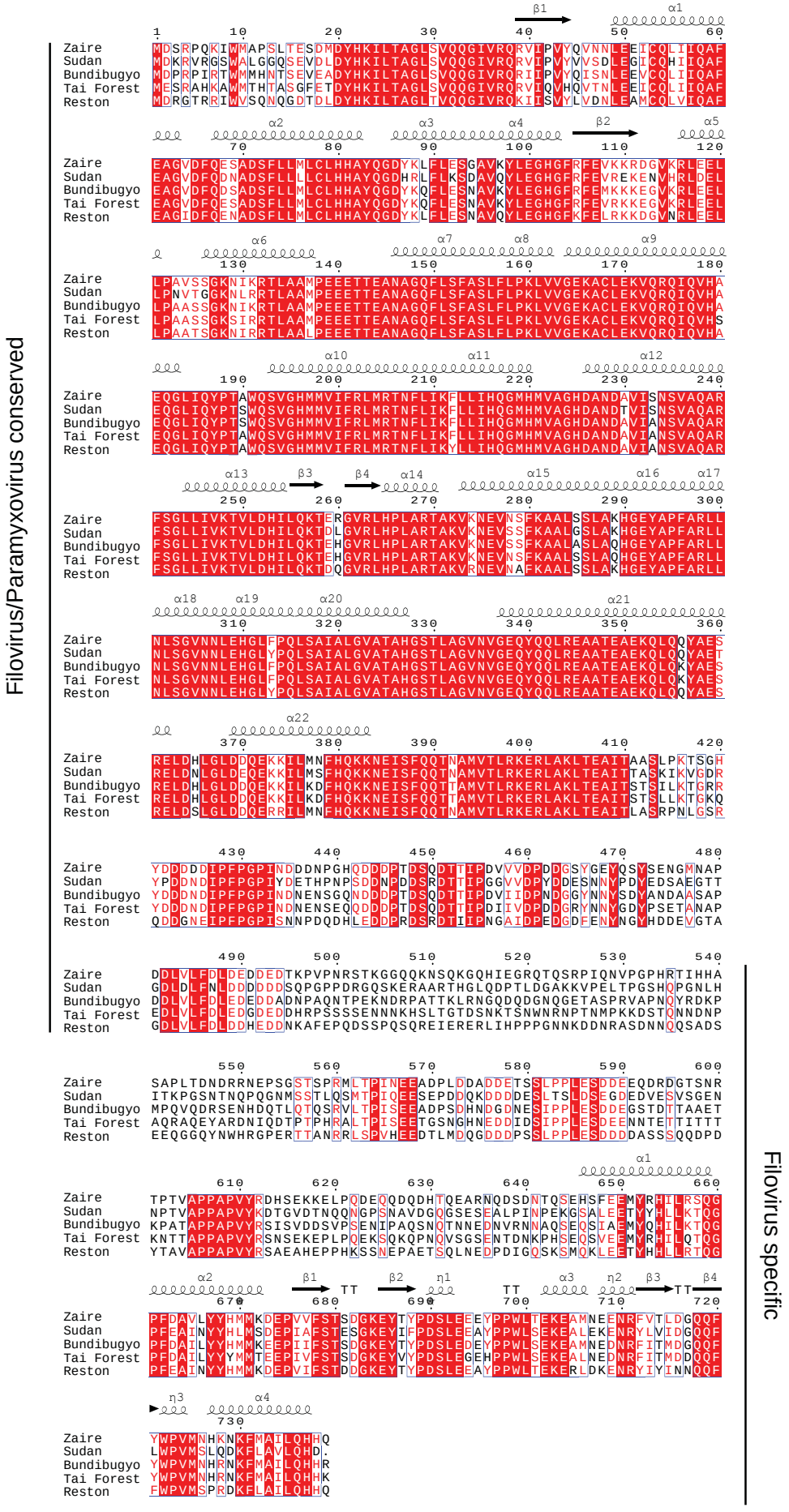

Figure S1, related to Figure 1 and 2 continued

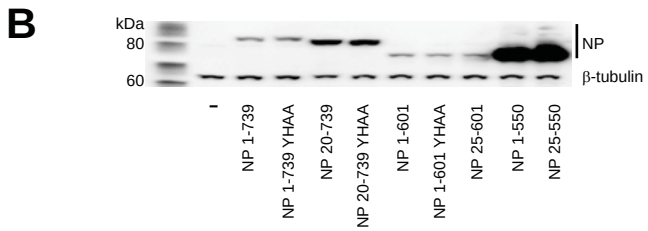

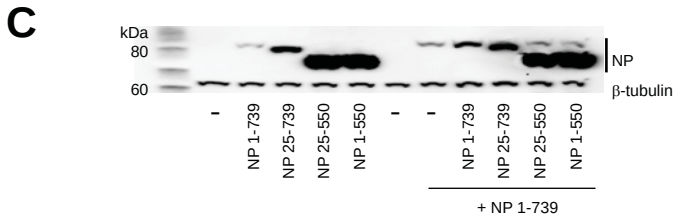

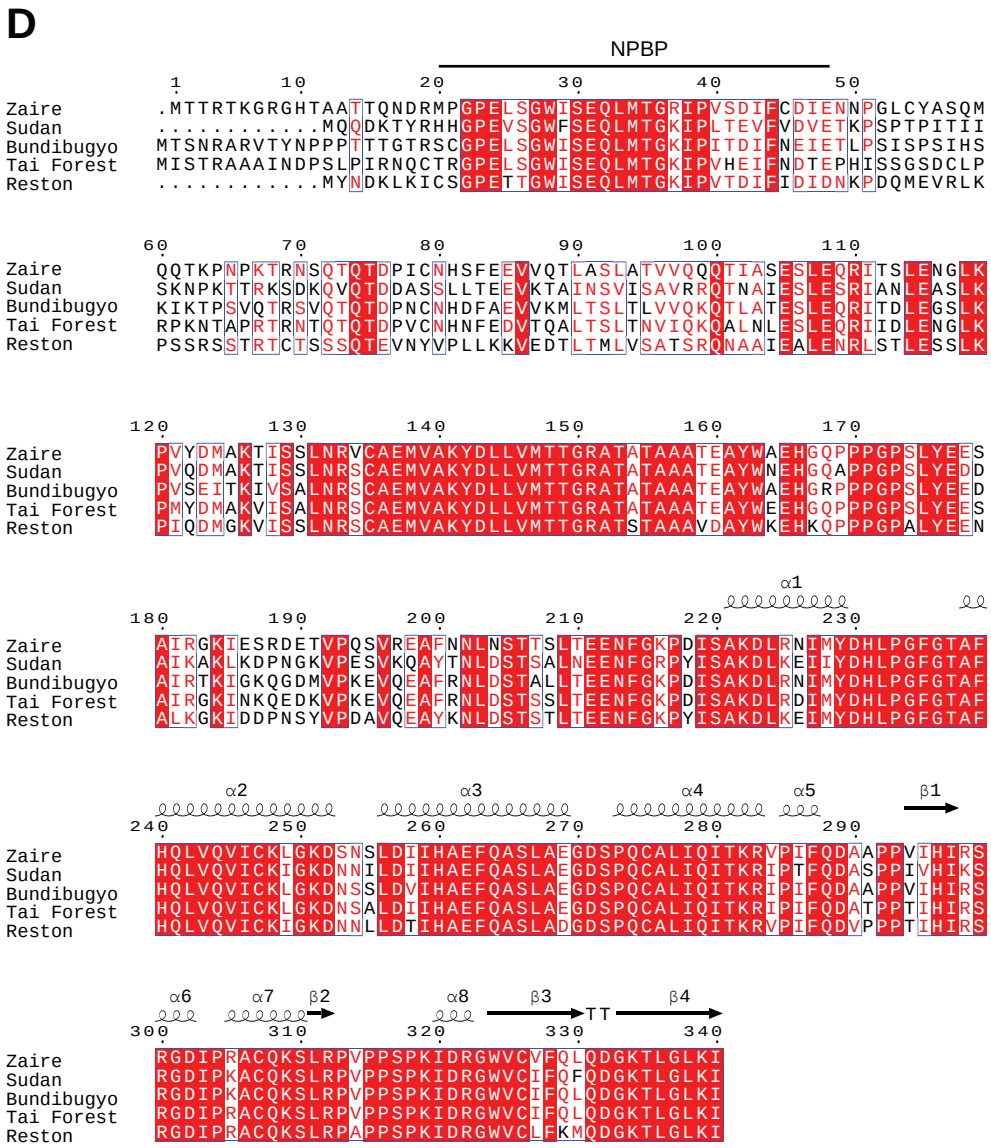

Figure S2, related to Figure 2 and 3

A

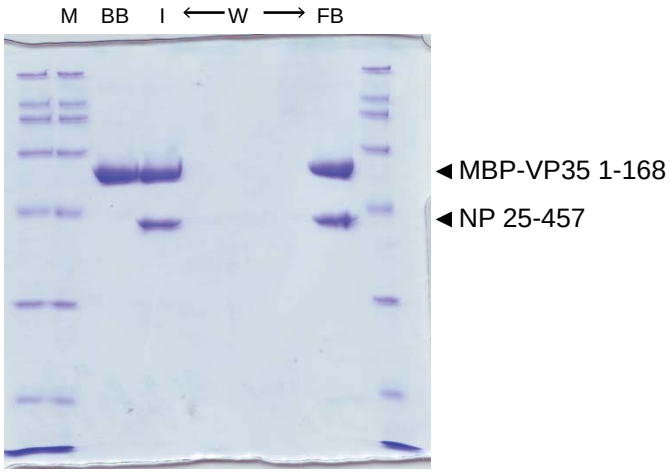

B

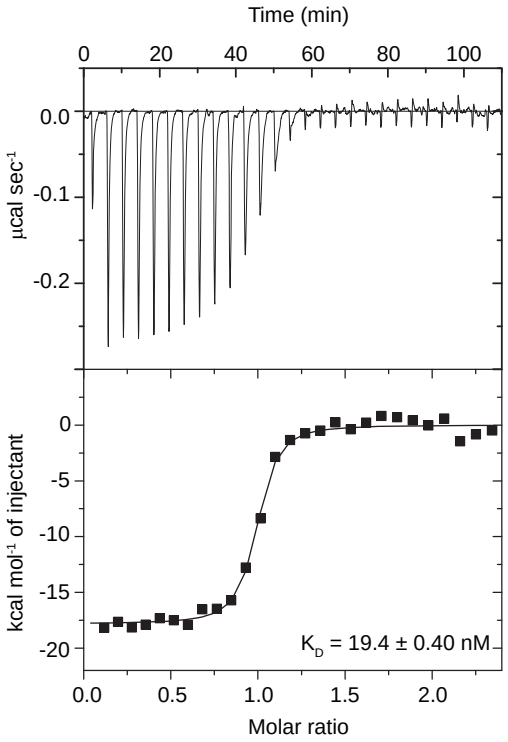

C

Summary of EBOV VP35 NPBP analysis

Construct	Sequence	Theoretical difference in BSA (Å²)*	K_D (nM)†	helical in TFE‡
VP35 20-48	20-MPGPELSGWISEQLMTGRIPVSDIFCDIE-48	0	28.9 ± 6.4	yes
VP35 26-48	26-SGWISEQLMTGRIPVSDIFCDIE	354	237± 49	yes
VP35 27-48	27-GWISEQLMTGRIPVSDIFCDIE	374	162 ± 25	yes
VP35 28-48	28-WISEQLMTGRIPVSDIFCDIE	392	215 ± 62	yes
VP35 29-48	29-ISEQLMTGRIPVSDIFCDIE	392	n.d.	no
VP35 30-48	30-SEQLMTGRIPVSDIFCDIE	426	n.d.	no
VP35 20-45	20-MPGPELSGWISEQLMTGRIPVSDIFC-45	63	2.18 ± 2.2	yes
VP35 20-44	20-MPGPELSGWISEQLMTGRIPVSDIF-44	94	7.83 ± 2.8	yes
VP35 20-43	20-MPGPELSGWISEQLMTGRIPVSDI-43	220	n.d.	yes
VP35 20-42	20-MPGPELSGWISEQLMTGRIPVSD-42	302	n.d.	yes

*Theoretical difference in buried surface area (BSA) values represent the sum of all deleted residues.

†K_D values were calculated from at least three independent ITC experiments. All experiments conducted in 150 mM NaCl.

‡Helical propensities in trifluoroethanol (TFE) were determined by CD measurements.

Figure S2, related to Figure 2 and 3 continued

D

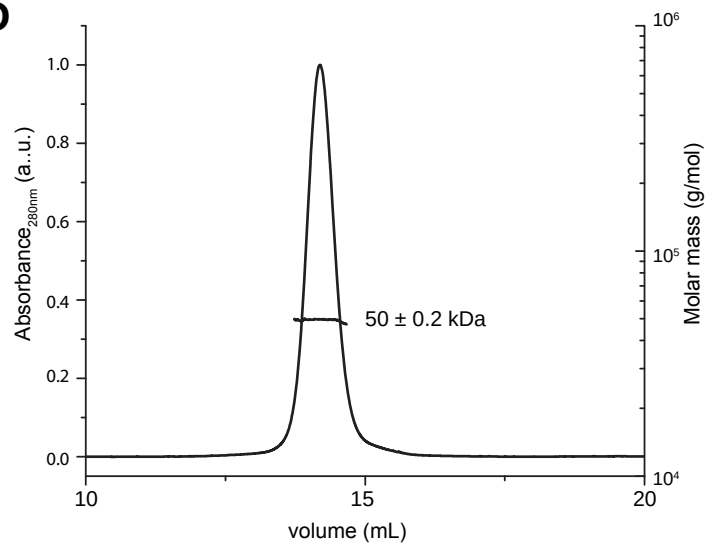

E

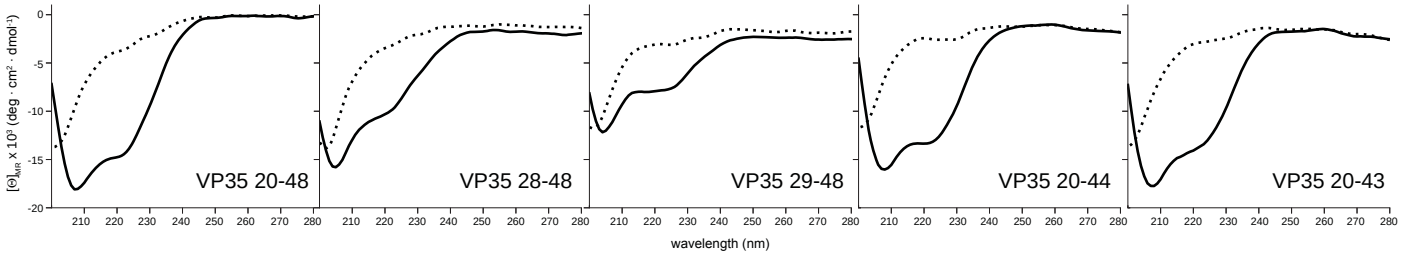

Figure S3, related to Figure 2, 3, 4

A

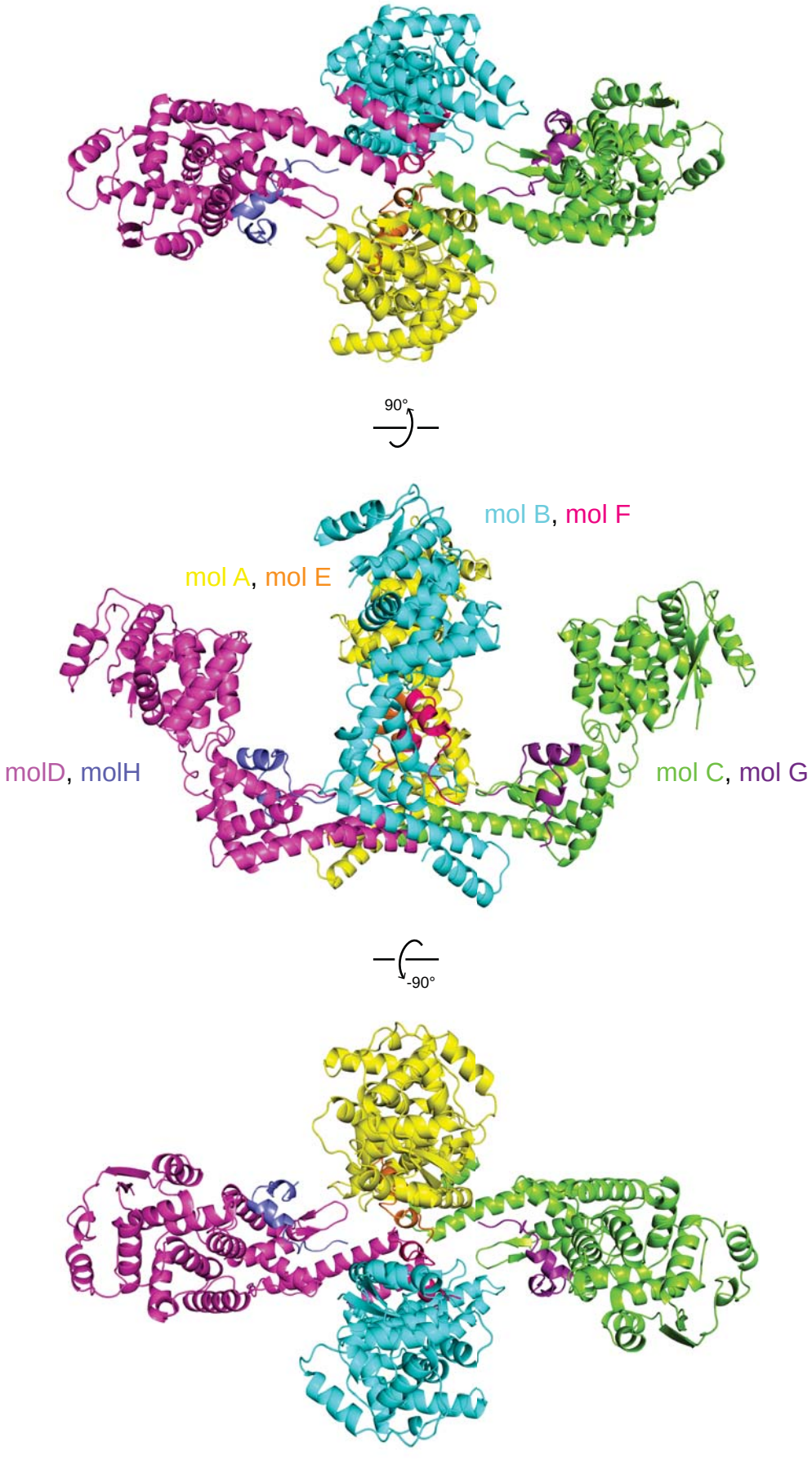

Figure S3, related to Figure 2, 3, 4 continued

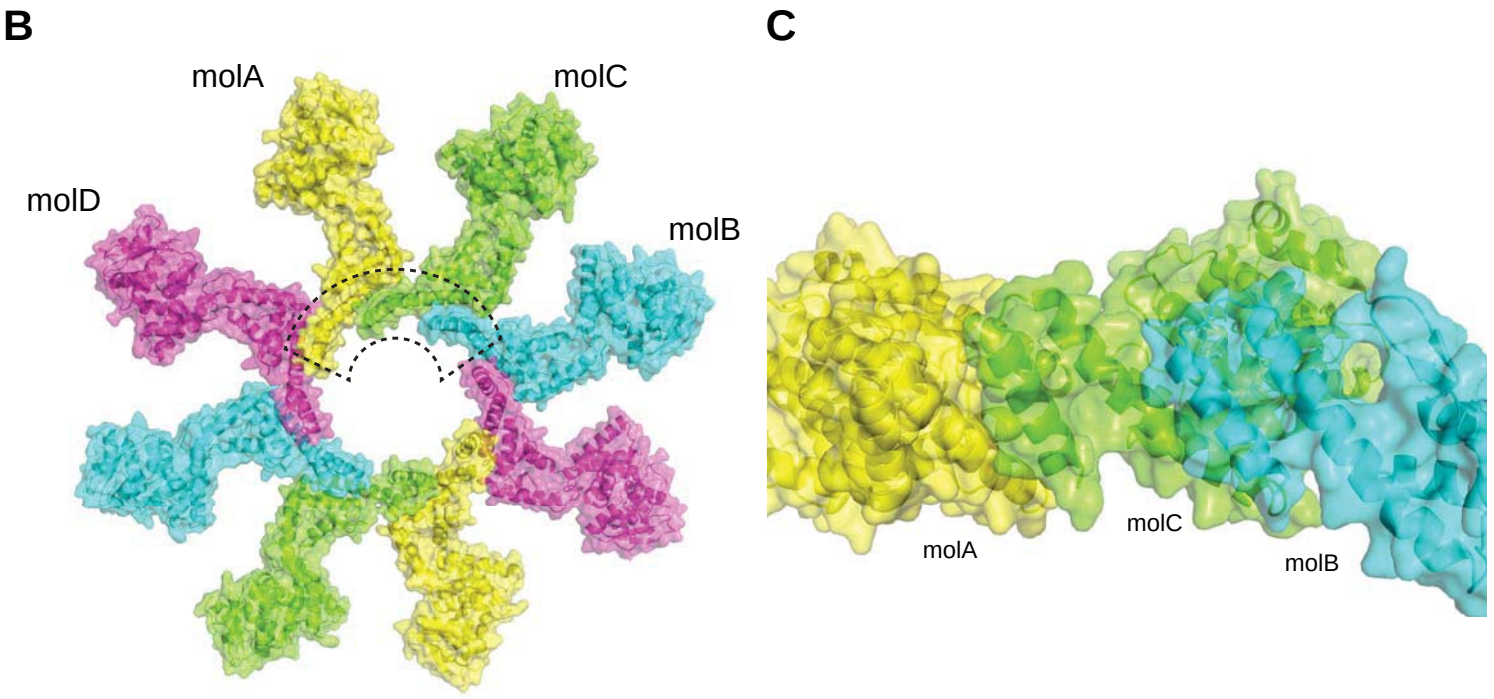

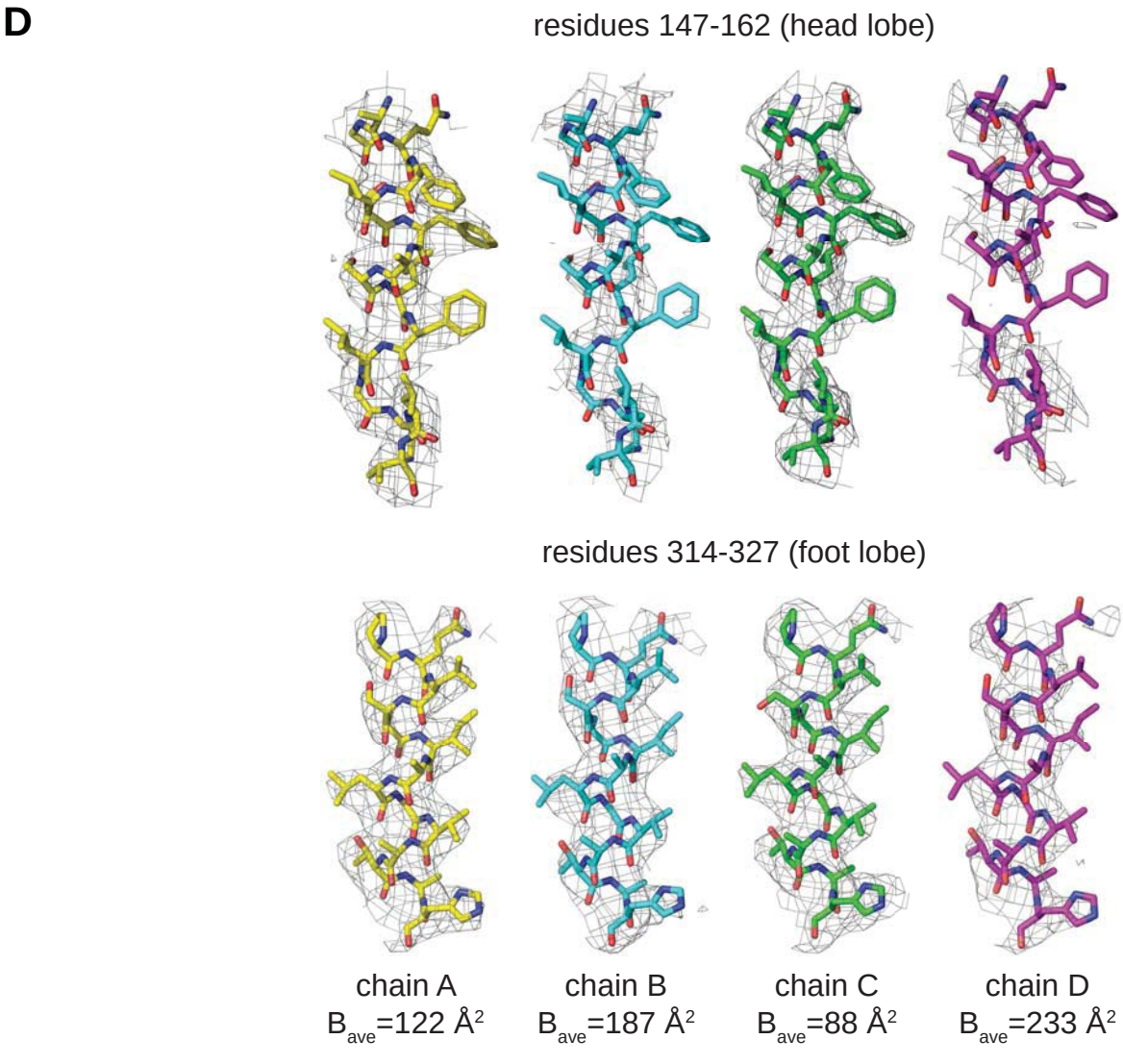

Figure S4, related to Figure 2, 3, 4

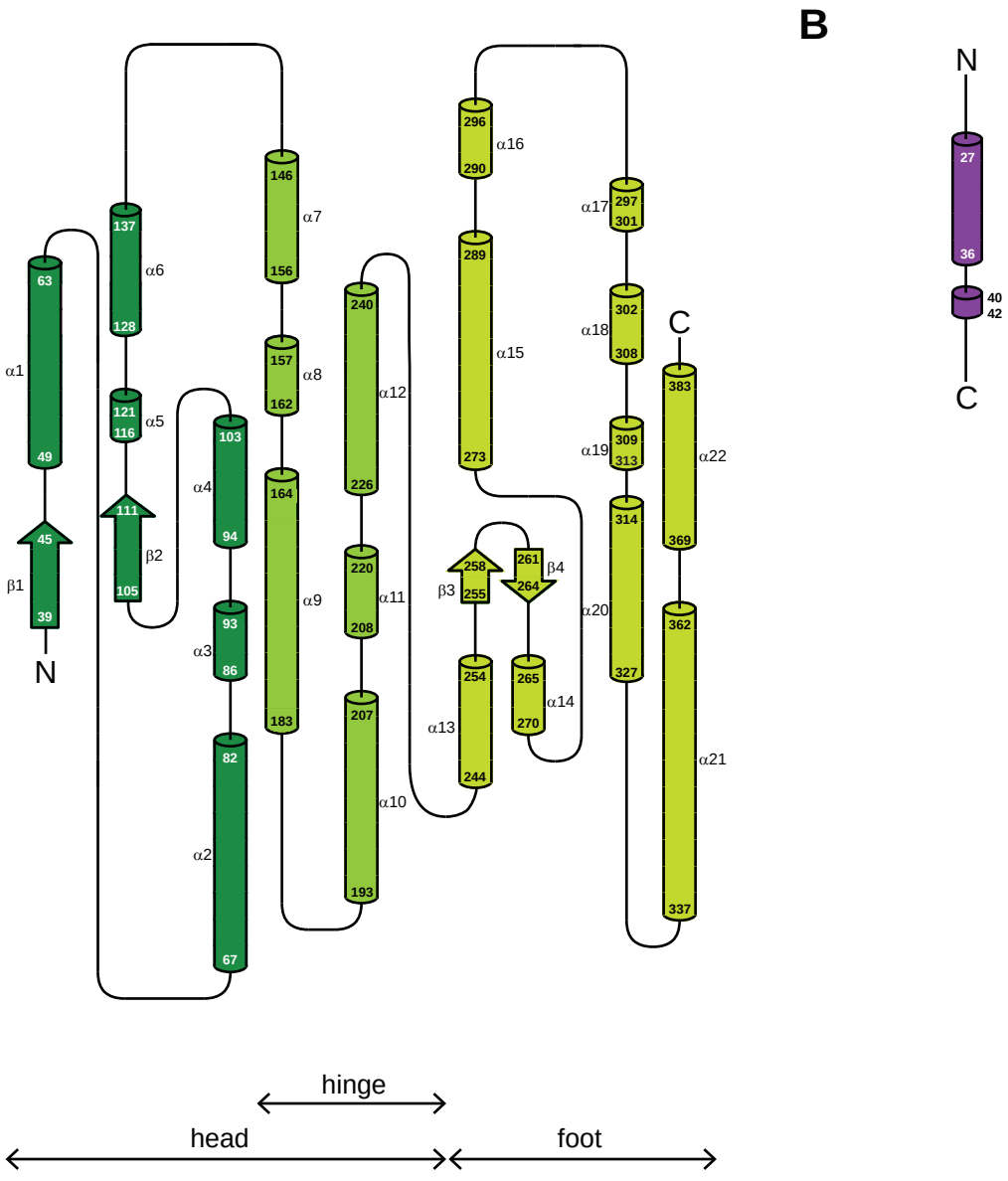

Figure S5, related to Figure 7

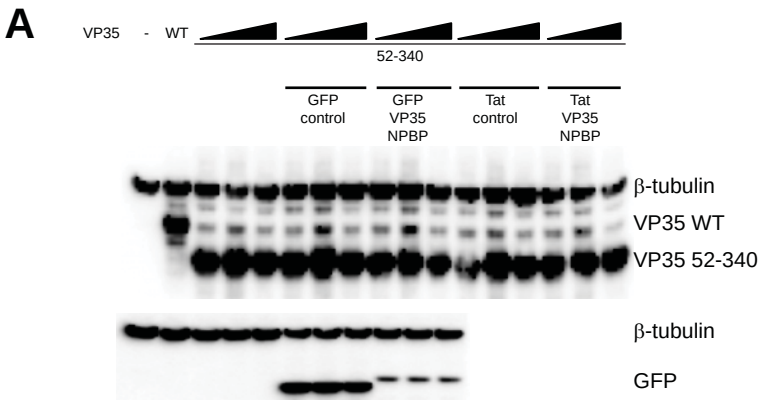

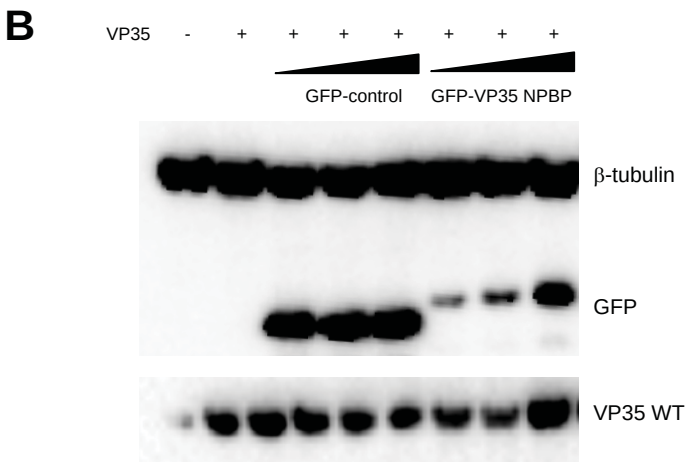

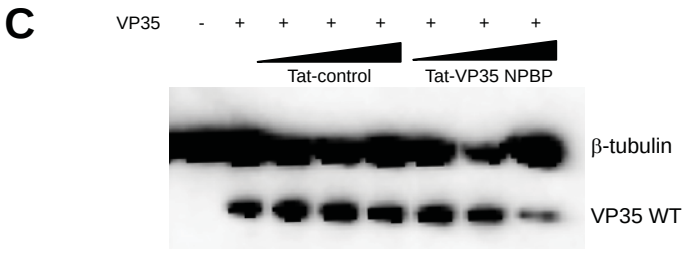

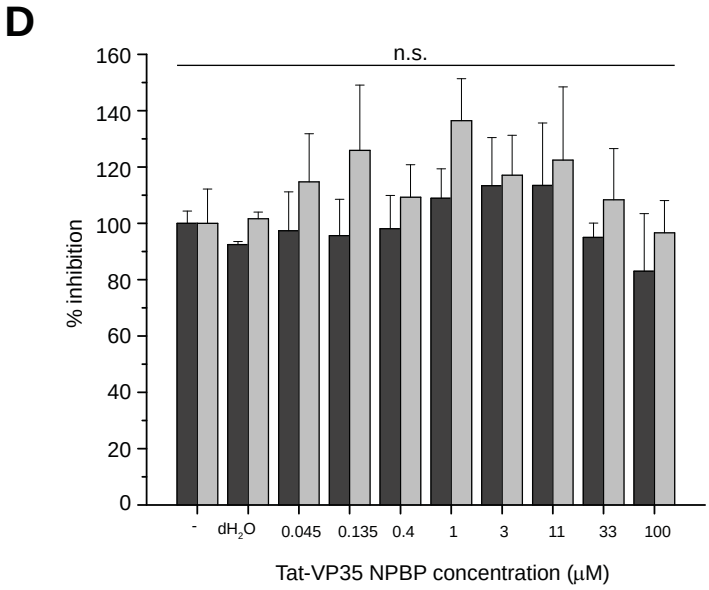

Figure S6, related to Figure 7

A

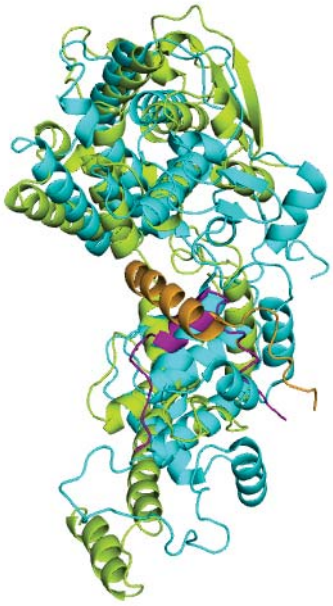

B

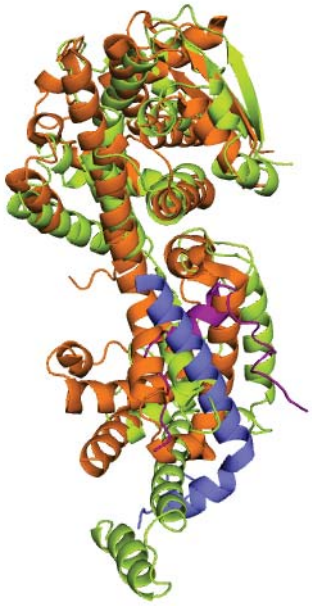

C

Structural alignment of the nucleoprotein N-terminal domain*

	VSV (residues 19-222)	Nipah (residues 32-258)	Rabies (residues 32-234)	RSV (residues 2-253)
EBOV (residues 37-240)	5.0 Å	5.1 Å	6.3 Å	4.7 Å
(aligned residues)	(144)	(176)	(136)	(176)

*PDB 3PMK, 3CO6, 2GTT, and 2WJ8 were used

REFERENCES

Chen, V.B., III, W.B.A., Headd, J.J., Keedy, D.A., Immormino, R.M., Kapral, G.J., Murray, L.W., Richardson, J.S., and Richardson, D.C. (2010). MolProbity: all-atom structure validation for macromolecular crystallography. Acta Crystallographica *D66*, 12-21.

Otwinowski, Z. and Minor, W. (1997). Processing of X-ray diffraction data collected in oscillation mode. Methods in Enzymology *276*, 307-326.